Stress drop at the Kephalonia Transform Zone estimated from the 2014 seismic sequence

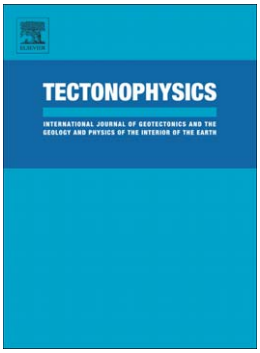

Stress drop at the Kephalonia Transform Zone estimated from the 2014 seismic sequence

Alessandro Caporali, Carine Bruyninx, Rui Fernandes, Athanassios Ganas, Ambrus Kenyeres, Martin Lidberg, Guenter Stangl, Holger Steffen, Joaquin Zurutuza

PII: S0040-1951(15)00603-4
DOI: doi: 10.1016/j.tecto.2015.11.004
Reference: TECTO 126830

To appear in: *Tectonophysics*

Received date: 16 October 2014
Revised date: 1 September 2015
Accepted date: 2 November 2015

Please cite this article as: Caporali, Alessandro, Bruyninx, Carine, Fernandes, Rui, Ganas, Athanassios, Kenyeres, Ambrus, Lidberg, Martin, Stangl, Guenter, Steffen, Holger, Zurutuza, Joaquin, Stress drop at the Kephalonia Transform Zone estimated from the 2014 seismic sequence, *Tectonophysics* (2015), doi: 10.1016/j.tecto.2015.11.004

Stress drop at the Kephalonia Transform Zone estimated from the 2014 seismic sequence

Alessandro Caporali[1)], Carine Bruyninx[2)], Rui Fernandes[3)], Athanassios Ganas[4)], Ambrus Kenyeres[5)], Martin Lidberg[6)], Guenter Stangl[7)], Holger Steffen[6)], Joaquin Zurutuza[1)]

1) Department of Geosciences, University of Padova, Italy

Email:alessandro.caporali@unipd.it; Tel. +39 (0)49 8279122

2)Royal Astronomical Observatory, Brussels, Belgium

3)University of Corvilha, Portugal

4) National Observatory of Athens, Greece

5)Satellite Geodetic Observatory FOMI, Budapest, Hungary

6) Lantmäteriet, Gävle, Sweden

7) BEV-OeAW, Graz, Austria

Abstract

The Kephalonia Transform Zone (KTZ) is a seismically active dextral transform fault decoupling the extensional deformed area of the Ionian Abyssal Plain and the compressional deformed area of the Mediterranean Ridge. We estimate a prominent steady state strain rate of 225±20 nstrain/year across the KTZ from the mean velocities of permanent Global Navigation Satellite System (GNSS) stations in East Italy and West Greece, which confirms previous estimates. Based on the regional statistical seismicity and using the local Gutenberg-Richter relation we investigate the energetic balance between stress accumulated as a consequence of the continuous dextral shear deformation, and the average stress released by shallow seismicity. If the maximum expected magnitude is M_w = 7.4, the estimated *a* and *b* parameters of the local Gutenberg-Richter relation and the geodetically determined shear-strain rate set an upper limit to the regional stress drop $\Delta\sigma \leq 0.4$ MPa.

We verify these values by analyzing a seismic sequence on the KTZ between January and February 2014, which culminated in the M_w= 6.09 event of Jan. 26, and the M_w= 6.14 event of Feb. 3. The estimated epicenters lie within a few kilometers from each other, on the western side of the Kephalonia Island, at a hypocentral depth ≤ 10 km. The measured coseismic displacements of GNSS stations in this area fit the expected surface dislocation, which can be predicted for an elastic half-space using the measured fault-plane solutions as input. If the hypocenters of the aftershocks are taken as indicator of optimal dextral shear-stress orientation, then a low regional deviatoric stress of 0.4 MPa, that is comparable with the maximum regional stress drop estimated above, is required for the Coulomb stress to match the pattern of the aftershocks of the 2014 sequence. As a consequence, we conclude that the regional deviatoric stress and the seismically released shear stress are in close balance in the KTZ seismic province.

1. Introduction

The Ionian Islands (Corfu, Lefkada, Ithaca, Kephalonia and Zante) in the Mediterranean lie in the transition zone between the westernmost termination of the Hellenic subduction, and the continental collision zone to the north (Figure 1; McKenzie, 1978; Le Pichon et al., 1995; Papazachos and Kiratzi, 1996; Shaw and Jackson, 2010). This transition zone, called the Kephalonia Transform Zone (KTZ), is a likely block boundary: the epicenters of the earthquakes tend to align along it and an offshore scarp is associated to the KTZ (Nyst and Thatcher, 2004; Reilinger et al., 2010). However, the gradient of velocity across this region (Figure 2) cannot be interpreted as the elastic response of a block to a fault that is slipping at depth beneath the Kephalonia fault. The length scale over which the velocity difference is expressed would require a locking depth of at least 80 km (i.e., the fault would penetrate through the subducting Nubian plate) and, to fit the amplitude of the velocity difference, the slip rate on such a fault would need to exceed 70 mm/yr (Floyd et al., 2010), a value that is not even close observed with modern geodetic techniques.

The KTZ is the structural element which explains the very different tectonic settings between the extensionally deformed area of the Ionian Abyssal Plain in the southwest and the compressional deformed area of the Hellenic Trench in the southeast (Figure 1). Compressive tectonics acts in the area east of this zone deforming the Plio–Quaternary, the Upper–Miocene and possibly the Mesozoic sediments (Kokinou et al., 2006).The high seismicity level in the Ionian Islands, one of the highest in the Aegean area (Papazachos and Papazachou, 1997), is a consequence of the active tectonics and crustal deformation. In addition, gravity data in the South Adriatic are consistent with a flexural model with an equivalent elastic thickness as low as 8 km. Such low values are typical of young continental regions (Maggi *et al.* 2000), and suggest that the area NW of Kephalonia is indeed continental.
A seismic sequence which occurred between January and February 2014 in the western part of Kephalonia Island fits to the picture described above (Papadopoulos et al., 2014). Two events of M_w> 6 occurred within 8 days in January - February 2014 with just a few kilometer distance in between. The position and magnitude of the accompanying sequence of aftershocks could accurately be recorded. In general, the area has a good record of historical seismicity (Votsi et al., 2011; Pondrelli et al., 2006). Furthermore, a dense network of Global Navigation Satellite System (GNSS) permanent sites in Italy and Greece allows the calculation of mean velocities based on multiyear tracking data. This enables the long-term strain rate across the KTZ to be accurately estimated. The large-scale fault geometry is also reasonably well known from previous investigations. Therefore, the main objectives of this paper are i) to combine the regional geodesy (long-term GNSS velocities), structural geology and statistical seismicity (regional Gutenberg Richter) data to obtain an estimate of the regional stress drop for the KTZ seismic province, and ii) to test this estimate using the 2014 events.

To achieve our first goal we present the available data (tectonics, statistical seismicity, regional strain rate from GNSS data) in Sections 2.1-2.3. The method of combination of these data is described in Sect. 3. We conclude Sect. 3 by pointing out that depending on the uncertainty on the Gutenberg Richter parameters 'a' and 'b' as well as on the maximum magnitude expected in this seismic province, the regional stress drop should have an upper limit ranging between 0.4 and 0.7 MPa.

We address our second goal in Sect. 4 by first reviewing (Sect. 4.1) the data available for the 2014 events: these are the published fault plane solutions and the coseismic displacement of GNSS sites

and InSAR reflector. The elastic Coulomb stress transfer is investigated in full detail in Sect. 4.2 and 4.3. We show that the regional deviatoric stress in the KTZ area as implied by the 2014 events is comparable with the upper limit to the stress drop set by the combination of statistical seismicity and GNSS-derived displacements.

2. Multidisciplinary Data

2.1 Fault orientation, length and maximum earthquake magnitude

The first clear seismological evidence for strike-slip motion in the Ionian Islands (Scordilis et al., 1985) comes from an analysis of the aftershocks of the Jan.17, 1983 (M_w=7.0) main shock. The Kephalonia segment of the KTZ was shown to strike in a NE–SW direction and to dip to the SE. Strike-slip faulting in this area has been further confirmed by fault-plane solutions (Anderson and Jackson, 1987; Papazachos et al., 1991), by waveform modeling (Kiratzi and Langston, 1991; Papadimitriou, 1993), by microseismicity studies (Hatzfeld et al., 1995) and geodetic measurements (Hollenstein et al., 2006, 2008; Kahle et al., 1996; Jenny et al., 2004; Caporali et al., 2011; Nocquet, 2012). North of the Kephalonia Island both the seismicity and the bathymetry change to a NNE direction. Stiros et al. (1994) suggested that the strong Aug. 12, 1953 event (m =7.2) occurred on the Kephalonia segment. They calculated the length of the fault be 85 km, its width 20 km and its slip rate equal to 2.7 cm/yr. These values are in good agreement with GNSS observations (Kahle et al., 1996). According to Papazachos and Papazachou (1997) the maximum magnitude for the Kephalonia segment should not exceed 7.4. This maximum magnitude also agrees with the magnitudes of the events of 1767, 1867, and 1953 when the entire segment ruptured. Waveform modeling of 10 strong earthquakes (m > 5) which occurred between 1981 and 1996 in the Kephalonia segment are all consistent with a dextral strike-slip fault with a thrust component, striking in a NE–SW direction and dipping to the southeast (Figure 1). Its typical focal mechanism has strike 38º, dip 63º and rake 172º.The Lefkada segment starts from the northern part of Kephalonia Island, strikes in a NNE–SSW direction and has a length of 40 km. This fault length corresponds to an earthquake magnitude 6.8 which is about the magnitude of the largest event that struck Lefkada during the last four centuries. The Lefkada segment is characterized by dextral strike-slip motion and the typical focal mechanism for an earthquake has strike 14º, dip 65º, rake 167º (Papazachos and Papazachou, 1997).

2.2 Regional strain rate from GNSS observations

Several GNSS permanent sites operate in Greece and Italy providing the necessary coverage for a continuous monitoring of the regional deformation. The analysis of the data is done as part of special projects and working groups within the EPN (European Permanent Network) of EUREF (Bruyninx et al., 2013) focusing on the maintenance and densification of the Reference Frame (Kenyeres,2014), of the velocity field and the crustal deformation (Lidberg et al., 2014). The GNSS data collection and analysis support the European project of a European Plate Observing System (EPOS). The analysis of the Greek and Italian sites is done on a weekly basis by the computing centers in Graz and Padova, based on the EPN processing standards.

The data used in this study start with GPS week 1632, ensuring full consistency with the IGb08 reference frame, satellite and receiver antenna models, GNSS final IGS orbits, satellite clocks and Earth Rotation Parameters. The processing is done with state-of-the-art software Bernese 5.2 (Dach et al., 2013) and is organized in seven daily sessions and one weekly combination by normal equation stacking. Minimum constraints are applied to Class A coordinates of selected sites of the EPN, ensuring proper alignment and scale, as well as reusability with other network solutions, e.g. global solutions, to mitigate network effects. The weekly solutions are eventually stacked to generate time series of coordinates in the IGb08 reference frame (Rebischung, 2012).
The velocities of the contributing GNSS sites predicted on the basis of a rigid rotation about the Euler Pole of Eurasia are subtracted from the velocities estimated in the IGb08 frame, to generate values in a frame co-rotating with the rigid Eurasian plate, which we refer to as the ETRF2000 frame. Permanent GNSS sites allow a systematic control of the monument stability, equipment, data flow and other environmental aspects which are crucial for the study of small signals requiring several years to be reliably detected. We show in Figure 1 the velocity data in the ETRF2000 frame for permanent GPS sites in the study area. The N-NE pattern in the Apulian block (Italy) associated with the counter rotation of the Italian Peninsula flips to S-SW across the Ionian, because the pattern of the velocities in the Greek part is dominated by the anticlockwise rotation of the Anatolian plate. As shown in the profile of interpolated velocities (Figure 2), the total velocity change is of the order of 40 mm/yr, and the point of steepest change, or maximum shear-strain rate, intersects the KTZ with an estimated slope of $\dot{\varepsilon}_g = 225 \pm 20$ nstrain yr^{-1} (1 nstrain = 10^{-9}). The velocity gradient is interpreted as distributed shearing across this part of western Greece, which is released by slip on a number of shallow faults (Floyd et al., 2010).

2.3 Statistical seismicity

The historical seismicity we have used is based on the Catalogue of Votsi et al. (2011) with 87 events of [5.2 ≤ m ≤ 7.4] from 1862 to 2008, and on the more recent Regional CMT Catalogue at the Istituto Nazionale di Geofisica e Vulcanologia (INGV) since 1997 (Pondrelli et al., 2006). The epicenters of these largest events are shown in Figure 3a. The cumulative distribution of the yearly number of events of magnitude greater than m [5.2 ≤ m ≤ 7.4] is shown in Figure 3b. From the estimated Gutenberg-Richter parameters a = 4.91 ± 0.04, b = -0.96 ± 0.07 one obtains the probability density of occurrence of an event of magnitude in the interval [m,m+dm] in terms of the parameters $a_s=a+log[-b* ln(10)]$ = 5.25 and $b_s=b$ = -0.96. Vamvakaris et al. (2013) proposed a new seismic zonation of the Aegean region in 113 seismic zones based on Catalogue data complete down to m=3.8 (1981). Their values of *a, b* for seismic zones S-C2 (Lefkada), S-C4 (W. Kephalonia) and S-C5 (E. Kephalonia) are in the interval [-0.99,-1.01] and [4.40, 5.14] for *b* and *a* respectively, where *a* is normalized to an area of 10000 km^2. Our study area is of comparable extension, so that our estimates can be considered consistent with Vamvakaris et al.'s (2013) to within one standard deviation.

3. Static regional stress drop

The geodetic strain rate measured by GNSS techniques is related to the present-day elastic energy stored in the rocks. The mechanical work done to displace crustal blocks along a fault during an earthquake releases part of this energy. Following the approach of Caporali et al. (2011) we express the Kostrov strain rate $\dot{\varepsilon}_S$ (Kostrov and Das, 1988) released by earthquakes in a given area in terms of the Gutenberg-Richter parameters (a_s, b_s) and empirical parameters expressing the rupture area *A(m)*, and the average displacement *u(m)* as functions of the magnitude m (Wells and Coppersmith, 1994):

$$\dot{\varepsilon}_S = \frac{1}{2}\frac{\int_{m_{min}}^{m_{max}} N(m)A(m)u(m)dm}{\int_{m_{min}}^{m_{max}} A(m)T(m)dm}. \quad (1)$$

The quantity *N(m)* is the yearly probability density of occurrence of an earthquake in the magnitude range [m, m+dm], and is expressed in terms of the parameters (a_s, b_s) in the familiar form

$$\log \mathrm{N(m)} = \mathrm{a_s} + \mathrm{b_s m}. \quad (2)$$

The quantity *T(m)* is the thickness of the seismogenic volume associated to an earthquake of magnitude m, and is related to the stress drop $\Delta\sigma$ and the average displacement *u(m)* by the equation

$$T(m) = \frac{\mu}{\Delta\sigma}u(m), \quad (3)$$

where μ is the shear modulus. The stress drop is assumed to be independent of magnitude.

Over the long-term and many earthquake cycles the Kostrov strain rate $\dot{\varepsilon}_S$ must have the geodetic strain rate $\dot{\varepsilon}_g$ as an upper limit. In such case Eq. (1) provides a constraint for the stress drop and the maximum magnitude, for a seismic province of known geodetic strain rate and statistical seismicity:

$$\Delta\sigma \leq \frac{2\mu\dot{\varepsilon}_g}{\mathrm{N}(m_{max})}\frac{b_s+b_{wc}}{b_{wc}}. \quad (4)$$

where $b_{WC}=b_{RA}+b_{AD}$ (WC stands for 'Wells and Coppersmith', RA stands for 'Rupture Area' and AD stands for 'Average Displacement'), and $m_{min}=0$. Equation (4) specifies how the available tectonic shear stress can be partitioned to individual events in a seismic province: for given strain rate and maximum magnitude a province with a larger a_s will have a smaller stress drop available than a province with a smaller a_s, for every magnitude below m_{max}. The equal sign corresponds to exact balance between buildup of elastic energy in the rocks and energy release through seismicity.

For the KTZ the parameters are all known. As shown in Figure 4, the maximum magnitude of 7.4 corresponds to a maximum stress drop of 0.38 MPa and raises to 0.74 MPa for an assumed maximum magnitude equal to the maximum observed magnitude plus 0.3, that is 7.7. This maximum stress drop is sensitive to changes of a_s and b_s, as exemplified in Figure 4.

The regional stress drop discussed above is an average quantity computed on the basis of catalogue data, regional geodetic strain rate and an assumed maximum magnitude. For individual earthquakes a dynamic stress drop is measured on the basis of the corner frequency of the power

spectrum of the radiated energy, and of a model of the fault shape, typically circular (Brune, 1970; Madariaga, 1976; Abercrombie,1995).For intraplate earthquakes in the Aegean area, typical values of the stress drop based on the Brune's approach are $\Delta\sigma$<3 MPa, according to Yolsal-Çevikbilen and Taymaz (2012) and Allmann and Shearer (2011), with a regional value of 0.5 MPa. A notable exception is represented by the M_w=6.4 Achaia - Elia event of 2008 in Western Peloponnesus (Ganas et al., 2009; Feng et al., 2010) where the stress drop is estimated as high as 5 MPa, but this is likely to be caused by an anomalously high rupture energy. For the Jan. 17, 1983 M=7.0 event near Kephalonia, Stavrakakis and Blionas (1990) report a stress drop of 1.4 MPa. One may expect that an average of the dynamic stress drops measured for individual earthquakes should be not larger than the regional stress drop we have estimated.

4. The seismic sequence of January/February 2014

The seismic sequence which struck the KTZ early in 2014 culminated with two events of M_w=6.09 and 6.14 on Jan.26 and Feb.3, respectively, with other events of M_w< 6. The hypocentral depth was fixed to 10 and 8 km for the two events and the epicenters were estimated within a few kilometers from each other. For these magnitudes the rupture area is of the order of 10 x 10 km^2. It is then reasonable to think that the second event was considerably influenced by the first. In the following subsections we analyze the KTZ 2014 sequence from three different viewpoints. First we use the information contained in the fault plane solutions to infer the surface displacement at GNSS sites, and compare the expected displacements with those measured by GNSS. Secondly, based again on the fault geometries inferred from the fault-plane solutions, the Coulomb stress on the receiver fault (the one activated on Feb. 3) is estimated on the basis of the radiation pattern of the Jan. 26 event. Thirdly, assuming the aftershocks as indicators of optimally oriented dextral strike-slip planes, we test if and to which extent the regional tectonic stress was relieved by these major seismic events. For these purposes the software package Coulomb 3.3 is used (Lin and Stein, 2004; Toda et al., 2005).

4.1 Epicenter location and coseismic surface displacements

The hypocenters of the entire sequence (main events and after shocks) have been re-located by Karasthathis et al.(2015) using an improved velocity model and a probabilistic approach. Relative to the coordinates published by the the INGV - RCMT (Regional CMT: http://autorcmt.bo.ingv.it/QRCMT-online/E1401262115A.html, http://autorcmt.bo.ingv.it/QRCMT-on-line/E1402030308A.html) they report a shift < 1 km in the NE direction, moving the events within the Kephalonia island but preserving the relative positions. Based on the analysis of InSAR data from the Cosmos Skymed and TanDEM satellites in conjunction with a single and double fault model Merryman Boncori et al. (2015) have obtained fault angles and magnitude estimates constrained by the SAR data. They concluded that both SAR-based models are in good agreement with the INGV solution.

The NOA (National Observatory of Athens) in Greece operates the permanent GNSS station VLSM in the Kephalonia Island, and two stations PONT and SPAN in the Lefkada Island. An additional station RLSO in the Peloponnesus may also be considered, but is probably too far away to have been affected by the 2014 seismic events. As shown by the discontinuities in the time series in

Figure 5 (daily estimates) and Table 1, VLSM was displaced in coincidence with the seismic events in the SW direction by a total of 16 mm South and 28 mm West. The individual events themselves caused each about 50% of the total displacement, being of very similar magnitude. The displacements on the surface of an elastic half space can be computed given the fault plane parameters. As shown in Figure 6, the measured displacements agree within three standard deviations with those predicted by the fault plane solutions, based on the Okada (1985) model, using the INGV fault plane solutions. The fault parameters of the INGV solution will be the basis for the numerical analyses in the rest of this section.

4.2 Stress transfer between the Jan. 26 and Feb. 3 events

The dual M_w=6.1 events provide an excellent test bed of the Coulomb failure criterion, where failure on the receiver fault (that of the Feb. 3 event) is promoted where the Coulomb stress change is positive:

$$\Delta\sigma_f = \Delta\tau_s + f\Delta\sigma_n. \quad (5)$$

Here, $\Delta\sigma_f$ is the change in failure stress on the receiver fault caused by slip on the source fault, $\Delta\tau_s$ is the change in shear stress (reckoned positive when sheared in the direction of fault slip), $\Delta\sigma_n$ is change in normal stress (positive if the fault is unclamped), and f is the effective coefficient of friction on the fault (King et al., 1994).

Figure 7 shows that failure on the fault of the Feb. 3 event (dip at 43°) was likely to be activated on the uppermost part of the fault plane, where an excess of approximately 0.5 MPa was received as a consequence of the Jan. 26 event (dip at 89°) on the source fault. The Coulomb stress change is computed on a preferred plane having the angles of the Feb. 3 event. The Coulomb stress change is contoured at depth intervals of 3 km, with the color scale in MPa. It should be emphasized that the above reasoning is based on assumed (i.e. not measured) hypocentral depths.

The assumed friction coefficient is f=0.36, for reasons discussed in the next subsection.

The red square in the bottom left part of Figure 7 corresponds to the estimated hypocenter of the M_w=5.5 event of Jan. 26 at 18:45 UTC, with a depth of 17 km (event E1401261845A in the INGV data base). Its location is associated with no particular Coulomb stress change. Hence it can be an example of an event which yielded because mature enough, without acceleration from the M_w=6.09 event of Jan. 26 at 13:55 UTC.

4.3 Aftershocks distribution, optimally oriented planes and energetic balance

It can be expected that under the regional tectonic stress preexisting joints and faults will be re-activated to form dip-slip faults at an angle β requiring the minimum tectonic stress. This angle is related to the coefficient of static friction f by the relation

$$\tan 2\beta = \frac{1}{f}. \quad (6)$$

The hypocenters of the aftershocks are likely to be located on these optimally oriented strike-slip planes. In our case Figure 8a shows that the aftershocks track very closely the strike of the KTZ at an azimuth approximately N30E. On the other hand the azimuth of the largest principal stress can be estimated to be 65° ± 5°. The angle β is comprised between the direction of the largest principal stress and the normal to the optimal plane, and is therefore 125° ± 5°. From eq. (6) it follows that the friction coefficient f is in the range [0.18, 0.58]. The angle 125° corresponds to a mean value f = 0.36, which is a typical value for strike-slip faults (Middleton and Copley, 2014).

In Figure 8 the cumulative Coulomb failure function resulting from both the Jan. 26 and Feb. 3 events on optimally oriented strike-slip faults is plotted for two different values of the regional stress: 10 MPa (Figure 8a) and 0.4 MPa (Figure 8b). The first value corresponds to a relatively large regional stress. The last value corresponds to the hypothesis that the regional deviatoric stress is low enough to equal the stress released on average by the local seismicity. Comparison with the distribution of the aftershocks clearly shows that the low regional stress hypothesis corresponds to an area of positive Coulomb stress which closely agrees with the distribution of the aftershocks. In this case of low regional stress, one can verify that the rotation of the shear axes near the fault is clearly visible. It is due to the local stress changes associated to the earthquakes prevailing over the regional stress. Away from the fault area the stress orientations are more regular.

5. Conclusions

Geodetic, structural and seismologic evidence support the concept that the KTZ is subject to a dextral shear-strain rate of as high as 225 ± 20 nstrain/yr. This deformation is accommodated by a seismic activity along the KTZ and the contiguous Lefkada Transform Zone. The size of the KTZ is such that M_w=7.4 can be considered an upper limit to the maximum expected magnitude. Comparison between the geodetically measured shear-strain rate and the seismically released shear-strain rate yields, for a given geodetic strain rate and maximum magnitude, an upper limit to the average regional stress drop in the range [0.4, 0.7] MPa, depending on the uncertainties in the Gutenberg Richter parameters and the maximum expected magnitude.

Further insight is now given by the dual events of Jan. 26 and Feb. 3, 2014, of M_w=6.09 and 6.14 respectively, and with hypocenters estimated within a few kilometers from each other. Coseismic offsets of the horizontal coordinates of permanent GNSS stations fit very well the expected surface deformation of an elastic half space, on the basis of the respective fault-plane solutions. An analysis of the Coulomb stress raised on the specific 'receiver' fault of the Feb. 3 event by the source fault of the Jan. 26 event shows that failure is likely to have started on the uppermost portion of the Feb. 3 event, for the assumed hypocenters.

Coulomb failure along specific directions for dextral strike-slips events can be described by the hypocenters of the aftershocks. From the period Jan. 26 to Mar.1, 2014 the aftershocks spread in the NE direction of the KTZ and tend to migrate away from the hypocenters of the largest events. Assuming a uniaxial stress regime with the largest principal stress at an azimuth of 65°, the acute angle from this direction to that of the aftershocks constrains the static friction coefficient to stay in the range [0.18,0.58], nominally f = 0.36. The distribution of the aftershocks at an average depth of 10 km is represented by an area of positive Coulomb stress provided that the regional stress is comparable with the static regional stress drop (see Sect. 3) of the order of 0.4 MPa. This is a

regional average value based on a steady state regime, in the sense that a Gutenberg Richter law resulting from a ca. 150 year seismic catalog and a strain rate from ca. 10 years of GPS data was assumed. Locally, for individual seismic events, the Coulomb stress change can be as much as four times larger or smaller. We tested an alternative regional stress of 10 MPa, and the increase of Coulomb stress in the regions populated by the aftershocks resulted smaller or negative. Hence the conclusion that the regional stress buildup due to regional tectonics, as inferred from the afterschock distribution, is comparable with the average release of seismic energy, from geodetic and historical data, and that the regional stress drop in the range [0.4, 0.7] MPa, for the given a_s, b_s of the regional Gutenberg-Richter relation, regional strain rate and maximum magnitude, should be a good approximation of the average stress released by the local seismicity at all magnitudes. The regional stress drop we have estimated for the KTZ seismic province should thus serve as reference to understand the dynamic stress drop released by individual earthquakes and independently measured based on the corner frequency of the spectrum of the radiated energy.

Acknowledgments.

The questions and suggestions of the Editor and of two Reviewers helped in improving a first draft of the manuscript. AC and JZ gratefully acknowledge the support of the Dipartimento Ambiente e Territorio of Regione del Veneto.

References

Abercrombie, R., 1995. Earthquake source scaling relationships from -1 to 5 ML using seismograms recorded at 2.5 km depth. *J. Geophys. Res.***100**, 24,015– 24,036.

Allmann, B. P., and P. M. Shearer, 2009. Global variations of stress drop for moderate to large earthquakes.*J. Geophys. Res.***114**, B01310, doi:10.1029/2008JB005821

Anderson, H., and J. Jackson, 1987. Active tectonics of the Adriatic region. *Geophys. J. R. Astron. Soc.***91**, 937–983.

Brune, J. N., 1970. Tectonic stress and the spectra of seismic shear waves from earthquakes. *J. Geophys. Res.***75**, 4997-5009.

Bruyninx, C., Altamimi, Z., Caporali., A., Kenyeres, A., Stangl, G., and Torres, J.A., 2013. Guidelines for EUREF Densifications, vers.5, available online at ftp://epncb.oma.be/pub/general/Guidelines_for_EUREF_Densifications.pdf.

Caporali, A., Aichhorn, C., Becker, M., Fejes, I., Gerhatova, L., Gitau, D., Grenerczy, G., Hefty, J., Krauss, S., Medac, D., Milev, G., Mojzes, M., Mulic, M., Nardo, A., Pesec, P., Rus, T., Simek, J., Sledzinski, J., Solaric, S., Stangl, G., Vespe, F., Virag, G., Vodopivec, F., and Zablotski, F., 2009. Surface kinematics in the Alpine-Carpathian-Dinaric and Balkan region inferred from a new multi-network GPS combination solution. *Tectonophysics* **474**, 295–321, doi: 10.1016/j.tecto.2009.04.035.

Caporali, A., S. Barba, M. M. C. Carafa, R. Devoti, G. Pietrantonio, and F. Riguzzi, 2011. Static stress drop as determined from geodetic strain rates and statistical seismicity. *J. Geophys. Res.* **116**, B02410, doi:10.1029/2010JB007671.

Dach, R., Hugentobler, U., Fridez, P., and Meindl, M., 2013. Bernese GPS Software 5.2 vers. 2013-07-18, available at http://www.bernese.unibe.ch/.

Feng,L., Newman, A.V., Farmer,G.T., Psimoulis, P., and Stiros, S.C., 2010.Energetic rupture, coseismic and post-seismic response of the 2008 M_w 6.4 Achaia-Elia Earthquake in northwestern Peloponnese, Greece: an indicator of an immature transform fault zone. *Geophys. J. Int.* **183**, 103–110, doi: 10.1111/j.1365-246X.2010.04747.x.

Floyd, M. A., H. Billiris, D. Paradissis, G. Veis, A. Avallone, P. Briole, S. McClusky, J.-M. Nocquet, K. Palamartchouk, B. Parsons, and P. C. England, 2010. A new velocity field for Greece: Implications for the kinematics and dynamics of the Aegean.*J. Geophys. Res.* **115**, B10403, doi:10.1029/2009JB007040.

Ganas, A., Serpelloni, E., Drakatos, G., Kolligri,M., Adamis, I., Tsimi,Ch. and E. Batsi, 2009.The M_w 6.4 SW-Achaia (Western Greece) Earthquake of 8 June 2008: Seismological, Field, GPS Observations, and Stress Modeling. *J. Earthq. Engin.* **13**(8), 1101-1124 doi:10.1080/13632460902933899.

Ganas, A., Oikonomou, A.I. and C. Tsimi, 2013. NOAFAULTS: A digital database for active faults in Greece. Bulletin of the Geological Society of Greece, vol. XLVII 2013. Proceedings of the 13th International Congress, Chania, Sept. 2013.

Hatzfeld, D., Kassaras, I., Panagiotopoulos, D., Amorese, D.,Makropoulos, K., Karakaisis, G., and Coutant, O., 1995. Microseismicity and strain pattern in northwestern Greece. *Tectonics* **14**, 773–785.

Hollenstein, Ch., Geiger, A., Kahle, H.-G. and Veis, G., 2006. CGPS time series and trajectories of crustal motion along the West Hellenic Arc. *Geophys. J. Int.* **164**(1), 182–191, doi:10.1111/j.1365-246X.2005.02804.x.

Hollenstein, Ch., Muller, M.D., Geiger, A. and Kahle, H.-G., 2008. Crustal motion and deformation in Greece from a decade of GPS measurements, 1993–2003, *Tectonophysics,* **449,** 17–40,doi:10.1016/j.tecto.2007.12.006.

Jenny, S., Goes, S., Giardini, D., and Kahle, H.G., 2004. Earthquake recurrence parameters from seismic and geodetic strain rates in the Eastern Mediterranean. *Geophys. J. Int.* **157**, 1331-1347, doi: 10.1111/j.1365-246X.2004.02261.x.

Kahle, H., Müller, M., and Veis, G., 1996. Trajectories of crustal deformation of Western Greece from GPS observations 1989– 1994. *Geophys. Res. Lett.* **23**, 677–680.

Kanamori, H., and D. L. Anderson, 1975. Theoretical basis of some empirical relations in seismology. *Bull. Seismol. Soc. Am.***65**(5), 1073-1095.

Karasthathis, V.K., Mouzakiotis, E., Ganas, A., and G. A. Papadopoulos, 2015. High-precision relocation of seismic sequences above a dipping Moho: the case of the January – February 2014 seismic sequence on Cephalonia Island (Greece). Solid Earth, 6, 173-184,2015, www.solid-earth.net/6/173/2015/doi:10.5194/se-6-173-2015

Kenyeres, A., 2014.European Dense Velocity Field Based on the Integration of the National Active GNSS Network Products, Paper presented at the 2014 EUREF Symposium, available online http://www.euref.eu/symposia/2014Vilnius/03-07-Kenyeres.pdf.

King, G.C.P., Stein, R.S., and Lin, J., 1994. Static stress changes and the triggering of earthquakes: *Bull. Seismol. Soc. Am.* **84** (3), 935-953.

Kiratzi, A., and Langston, C., 1991. Moment tensor inversion of the 1983 January 17 Kefallinia event of Ionian islands (Greece). *Geophys. J. Int.* **105**, 529–535.

Kokinou,E., Papadimitriou, E.,Karakostas,V.,Kamberis, E.,and Vallianatos,F., 2006. The Kephalonia Transform Zone (offshore Western Greece) with special emphasis to its prolongation towards the Ionian Abyssal Plain. *Mar. Geophys. Res.* **27**, 241–252,doi:10.1007/s11001-006-9005-2.

Kostrov, B.V., and Das, S., 1988. Principles of Earthquake Source Mechanics. Cambridge University Press, Cambridge, UK, 286 pp.

Le Pichon, X., N. Chamot-Rooke, S. Lallemant, R. Noomen, and G. Veis (1995), Geodetic determination of the kinematics of central Greece with respect to Europe: Implications for eastern Mediterranean tectonics, J. Geophys. Res., 100(B7), 12,675–12,690, doi:10.1029/95JB03170.

Lidberg, M., Altamimi, Z., Bruyninx, C., Caporali, A., Dousa, J., Fernandes, R.M., Kenyeres, A., Stangl, G., and Steffen, H., 2014. The EPN Working Group on Deformation Models, Paper presented at the 2014 EUREF Symposium, available online http://www.euref.eu/symposia/2014Vilnius/03-01-Lidberg.pdf.

Lin, J. and R.S. Stein, 2004. Stress triggering in thrust and subduction earthquakes, and stress interaction between the southern San Andreas and nearby thrust and strike-slip faults. *J. Geophys. Res.* **109**, B02303, doi:10.1029/2003JB002607.

Louvari, L.,Kiratzi, A.A. and B.C. Papazachos, 1999.The Cephalonia Transform Fault and its extension to western Lefkada Island (Greece). *Tectonophysics* **308**, 223–236.

Madariaga, R., 1976. Dynamics of an expanding circular fault. *Bull. Seismol. Soc. Am.* **66**, 639-666.

Maggi, A., Jackson, J.A., McKenzie, D. and Priestley, K., 2000. Earthquake focal depths, effective elastic thickness, and the strength of the continental lithosphere. *Geology* **28,** 495–498.

McKenzie, D.,1978. Active tectonics of the Alpine-Himalayan belt—Aegean Sea and surrounding regions. *Geophys. J. R. Astron. Soc.* **55**(1), 217–254.

Merryman Boncori, J.P., Papoutsis, I., Pezzo, G., Tolomei, C., Atzori, S., Ganas, A., Karastathis, V., Salvi, S., Kontoes, C., Antonioli, A. ,2015. The February 2014 Cephalonia Earthquake (Greece): 3D Deformation Field and SourceModeling from Multiple SAR Techniques. Seismological Research Letters 86 (1), 124-137,doi: 10.1785/0220140126

Middleton, T.A. and A. Copley, 2014. Constraining fault friction by re-examining earthquake nodal plane dips. *Geophys. J. Int.* 196 (2), 671-680, doi: 10.1093/gji/ggt427

Nocquet, J.M., 2012. Present-day kinematics of the Mediterranean: A comprehensive overview of GPS results. *Tectonophysics 579, 220-242.*

Nyst, M., and W. Thatcher, 2004. New constraints on the active tectonic deformation of the Aegean. *J. Geophys. Res.* **109**, B11406, doi:10.1029/2003JB002830.

Okada, Y., 1985. Surface deformation due to shear and tensile faults in a half-space. *Bull. Seismol. Soc. Am.* **75**, 1135-1154.

Papadimitriou, E.E., 1993. Focal mechanisms along the convex side of the Hellenic Arc and its tectonic significance. *Boll. Geofis. Teor. Appl.* **140**, 401–426.

Papadopoulos, G. A., V. K. Karastathis, I. Koukouvelas, M. Sachpazi, I.Baskoutas, G. Chouliaras, A. Agalos, E. Daskalaki, G. Minidakis, A.Moshou, A. Mouzakiotis, K. Orfanogiannaki, A. Papageorgiou, D.Spanos, and I. Triatafylou, 2014. The Cephalonia, Ionian Sea (Greece), sequence of strong

earthquakes of January–February 2014: A first report, Res. Geophys. 4(1), doi:10.4081/rg.2014.5441

Papazachos, B.C., and Kiratzi, A., 1996. A detailed study of the active crustal deformation in the Aegean and surrounding area. *Tectonophysics* **253**, 129–153.

Papazachos, B.C., and Papazachou, C.C., 1997. The Earthquakes of Greece. Ziti Publication Co., Thessaloniki, 304 pp.

Papazachos, B., Kiratzi, A., and Papadimitriou, E., 1991. Regional focal mechanisms for earthquakes in the Aegean Area. *Pure Appl. Geophys.* **136**, 407–420.

Pondrelli, S., S. Salimbeni, G. Ekström, A. Morelli, P. Gasperini and G. Vannucci, 2006. The Italian CMT dataset from 1977 to the present. Phys. Earth Planet. Int. 159(3-4), 286-303, doi:10.1016/j.pepi.2006.07.008.

Rebischung, P., 2012: IGb08: an update on IGS08, IGSmail 6663, http://igscb.jpl.nasa.gov/pipermail/igsmail/2012/007853.html.

Reilinger, R., McClusky, S., Paradissis, D., Ergintav, S. and Vernant, P., 2010. Geodetic constraints on the tectonic evolution of the Aegean region and strain accumulation along the Hellenic subduction zone. *Tectonophysics,* **488,** 22-30, doi:10.1016/j.tecto.2009.05.027.

Scordilis, E.M., Karakaisis, G.F., Karakostas, B.G., Panagiotopoulos, D.G., Comninakis, P.E., and Papazachos, B.C., 1985. Evidence for Transform Faulting in the Ionian Sea: the Cephalonia Island Earthquake Sequence of 1983. *Pure Appl. Geophys.* **123**, 388–397.

Shaw, B. and J. Jackson, 2010. Earthquake mechanisms and active tectonics of the Hellenic subduction zone, *Geophys. J. Int.* **181**, 966–984, doi: 10.1111/j.1365-246X.2010.04551.x.

Stavrakakis, G. N. and Blionas, S. V., 1990. Source parameters of some large earthquakes in the eastern Mediterranean region based on an iterative maximum entropy technique. *Pure Appl. Geoph.* **132**(4), 679-698, doi: 10.1007/BF00876813.

Stiros, S., Pirazoli, P., Laborel, J., and Laborel-Deguen, F., 1994.The 1953 earthquake in Cephalonia (Western Hellenic Arc): coastal uplift and halotectonic faulting. *Geophys. J. Int.* **117**, 834–849.

Toda, S., R. S. Stein, K. Richards-Dinger and S. Bozkurt, 2005. Forecasting the evolution of seismicity in southern California: Animations built on earthquake stress transfer. *J. Geophys. Res.* **110**, B05S16, doi:10.1029/2004JB003415.

Vamvakaris D.A., C. B. Papazachos, C. Papaioannou, E. M. Scordilis, and G. F. Karakaisis, 2013. A detailed seismic zonation model for shallow earthquakes in the broader Aegean area. *Nat. Hazards Earth Syst. Sci. Discuss.* **1**, 6719–6784, doi:10.5194/nhessd-1-6719-2013.

Votsi, I., Tsaklidis, G.M., and Papadimitriou, E.E., 2011.Seismic Hazard Assessment in Central Ionian Islands Area (Greece) Based on Stress Release Models. *Acta Geophysica* **59**(4), 701-727,doi: 10.2478/s11600-011-0020-6.

Wells, D.L., and Coppersmith, K.J., 1994. New empirical relationships among Magnitude, Rupture Length, Rupture Width, Rupture Area and Surface Displacement. *Bull. Seismol. Soc. Am.* **84**, 974 – 1002.

Yolsal-Çevikbilen, S.,and T. Taymaz, T., 2012. Earthquake source parameters along the Hellenic subduction zone and numerical simulations of historical tsunamis in the Eastern Mediterranean. *Tectonophysics* **536–537**, 61–100.

Tables

GNSS Site	Long (deg)	Lat (deg)	East (m)	North (m)	Up (m)
PONT	20.59	38.62	-0.007	0.000	0.005
RLSO	21.46	38.06	-0.001	-0.003	0.001
SPAN	20.67	38.78	0.000	0.000	-0.004
VLSM	20.59	38.18	-0.028	-0.016	-0.011

Table 1.Coseismic offsets for selected permanent GNSS stations of the National Observatory of Athens (NOA), resulting from the comparison of the coordinates before Jan 26, 2014 and after Feb. 03, 2014. Uncertainties in the average coordinates of these sites before and after the seismic events are 0.003 m for horizontal and 0.009 m for vertical (3σ).

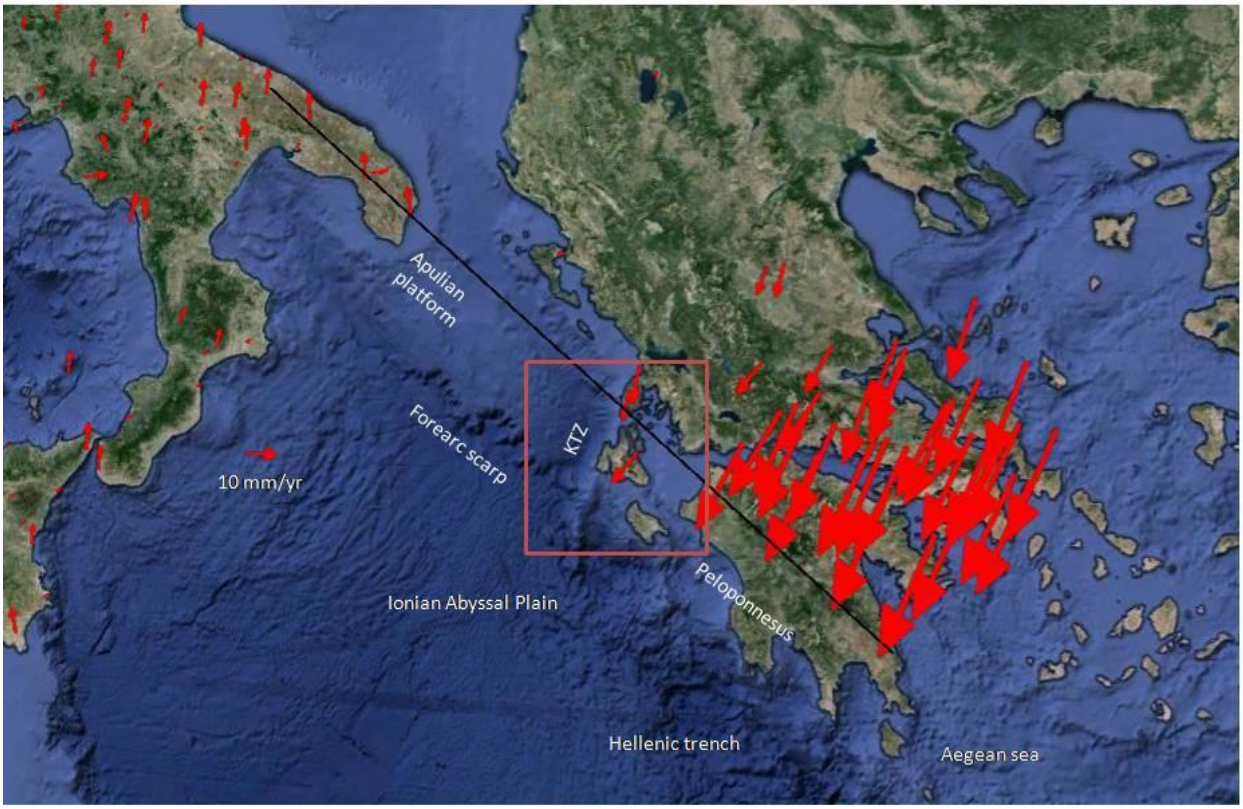

Figure 1. The study area, with seafloor topography as a guide to identify continental collision (NW), oceanic subduction (SE) and the intervening decoupling area (KTZ) accommodating a dextral shear stress. The velocities of permanent GPS sites highlight the kinematics of the area in the ETRF2000 reference frame co-moving with continental Eurasia: the NE motion of Apulia and an anticlockwise rotation of the Anatolian plate result in a dextral shear strain on the KTZ. The interpolation of the velocities to the profile (black line) through the KTZ is shown in Figure 2. Uncertainties in the velocities are typically 0.5 mm/yr (1σ). The rectangle defines the study area.

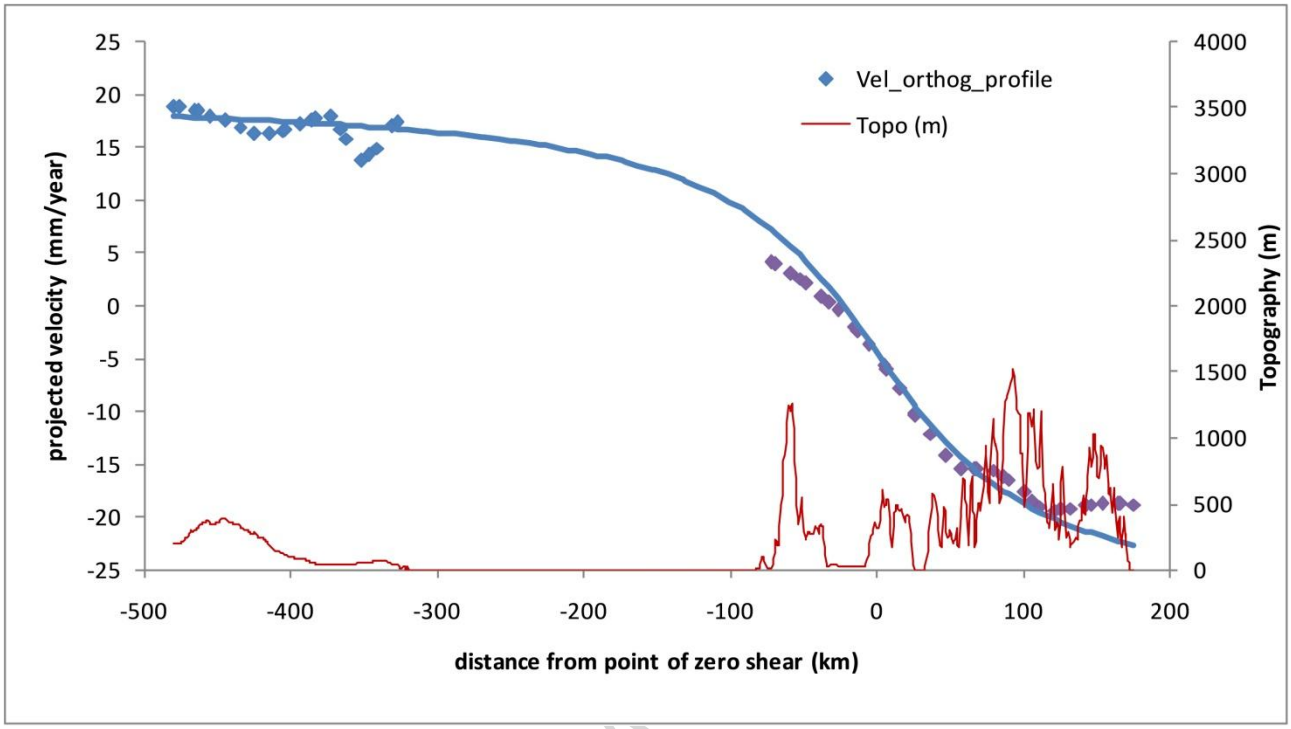

Figure 2.Interpolated velocity change from the GPS sites shown in Figure 1 along the profile across the KTZ. The steepest point very well agrees with the location of the KTZ. Topographic profile is based on GTOPO30 data of National Oceanic and Atmospheric Administration (NOAA).

(a)

(b)

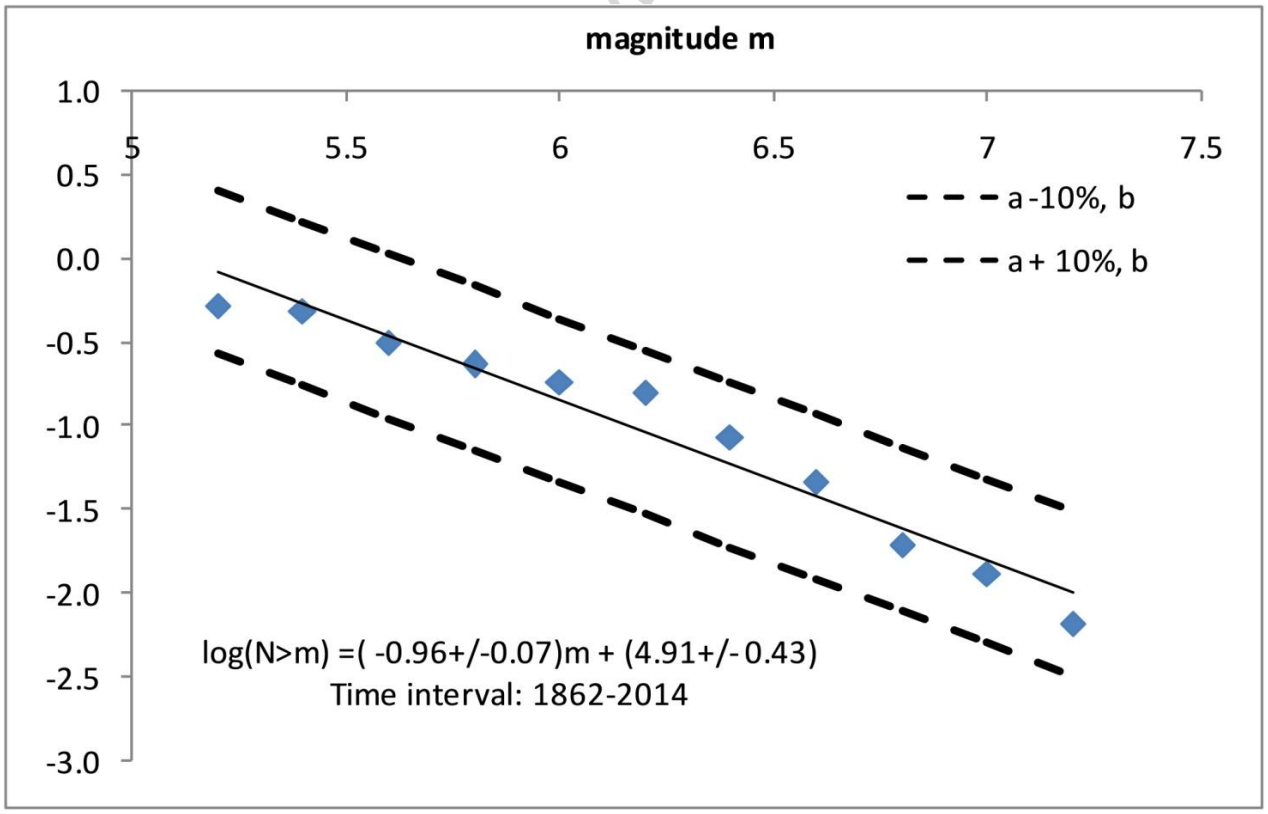

Figure 3. (a) Location of the 84 earthquakes in the KTZ area and in the time interval 1862 -2014 used for the construction of the regional Gutenberg-Richter relation. Faults are taken from the database of Ganas et al. (2013). (b) Gutenberg-Richter relation for the catalogue earthquakes, with the ±10% band of uncertainty of the parameter *a* (dashed lines) and the best fitting regression line (continuous line). Uncertainties in the a,b parameters are 1σ least squares standard deviations.

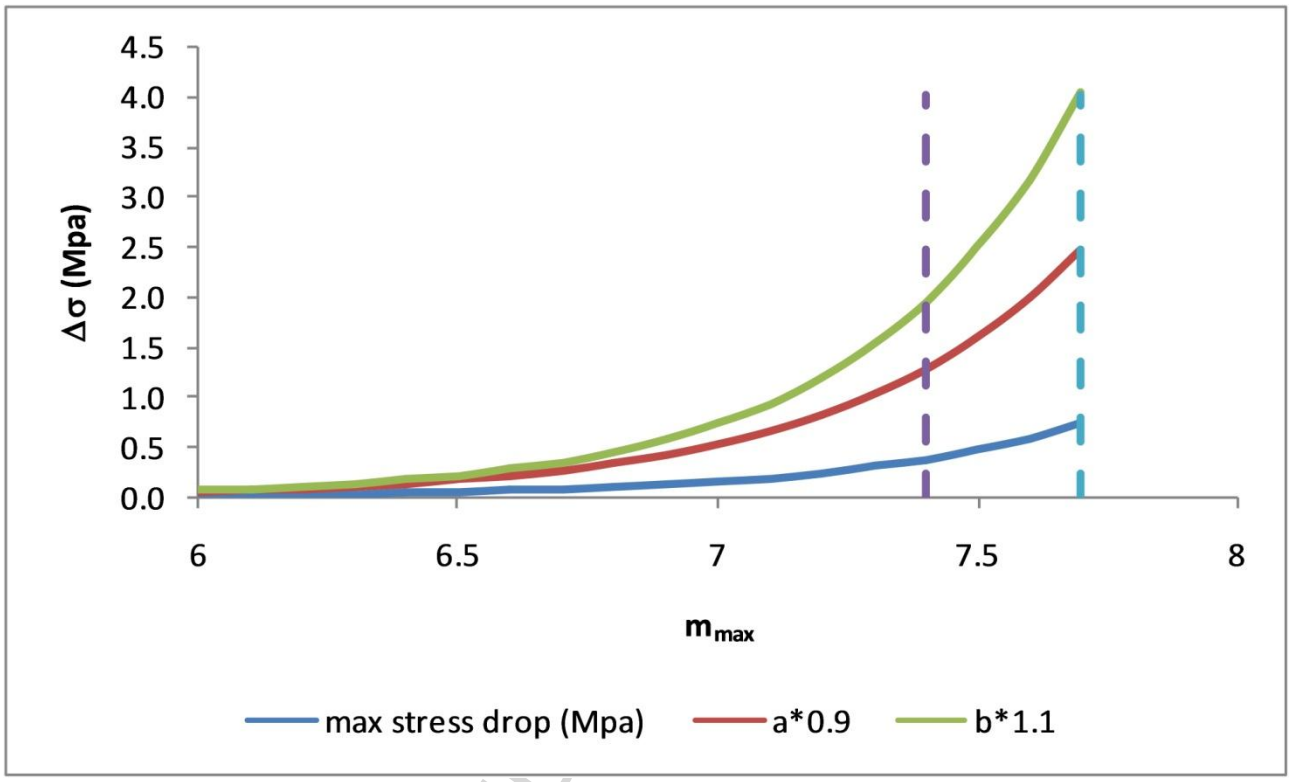

Figure 4. Bounding curves for the regional stress drop computed from historical seismicity and geodetic shear-strain rate, as a function of the maximum expected magnitude. The vertical dashed lines correspond to M_{max}=7.4 and 7.7. The sensitivity of the maximum stress drop on the a_s and b_s parameters of the Gutenberg-Richter probability density function is also exemplified by showing the change in the curve when the parameters are changed.

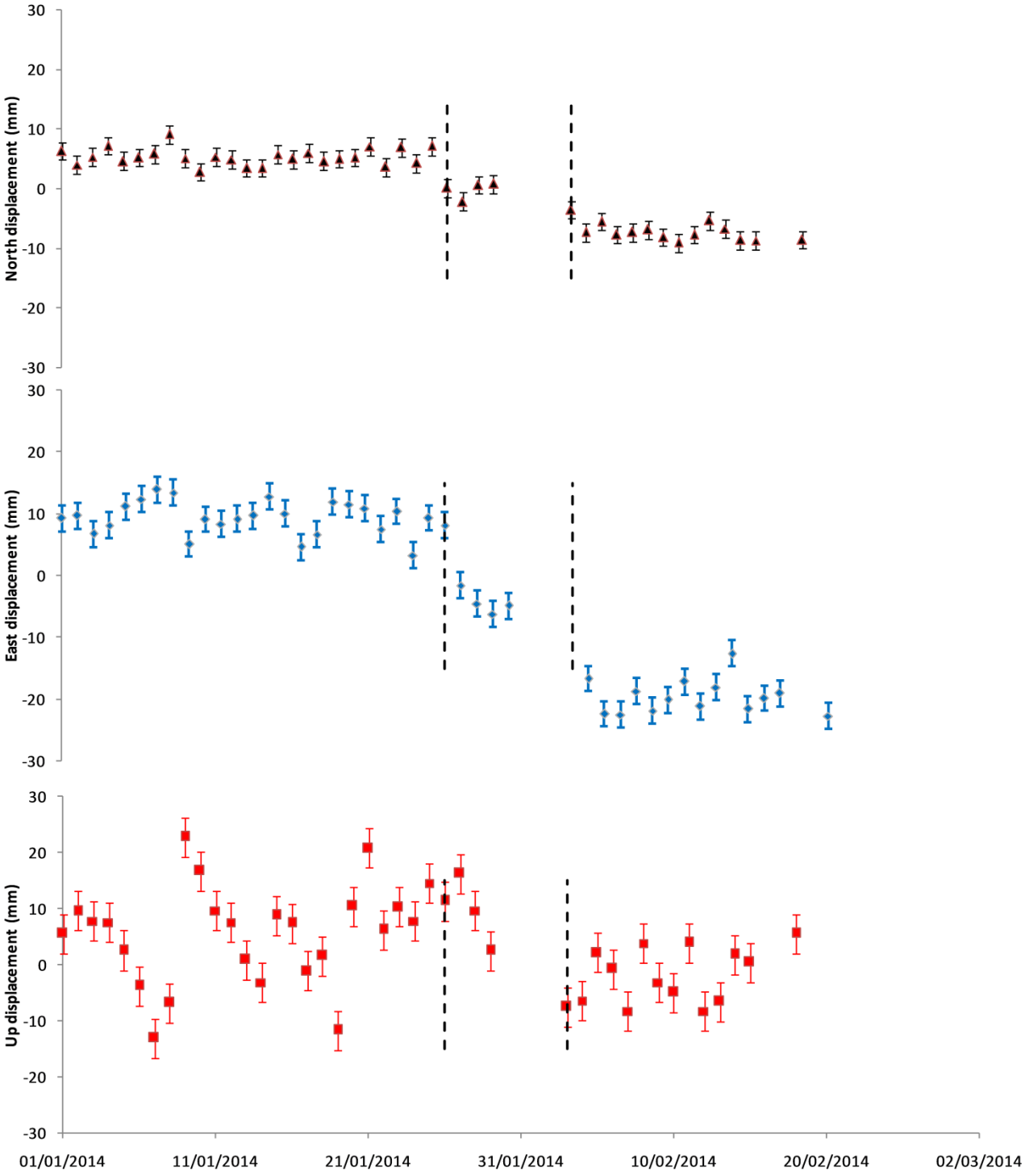

Figure 5. Time series of daily estimates of the position of the permanent GNSS station VLSM, a few kilometer off the epicenter of the Jan. 26 M_w=6.09 and Feb. 03 M_w=6.14 events, showing the successive position changes of the antenna in coincidence with the earthquakes. The epochs of the two events are marked by vertical dashed lines. Error bars represent 1σ uncertainties.

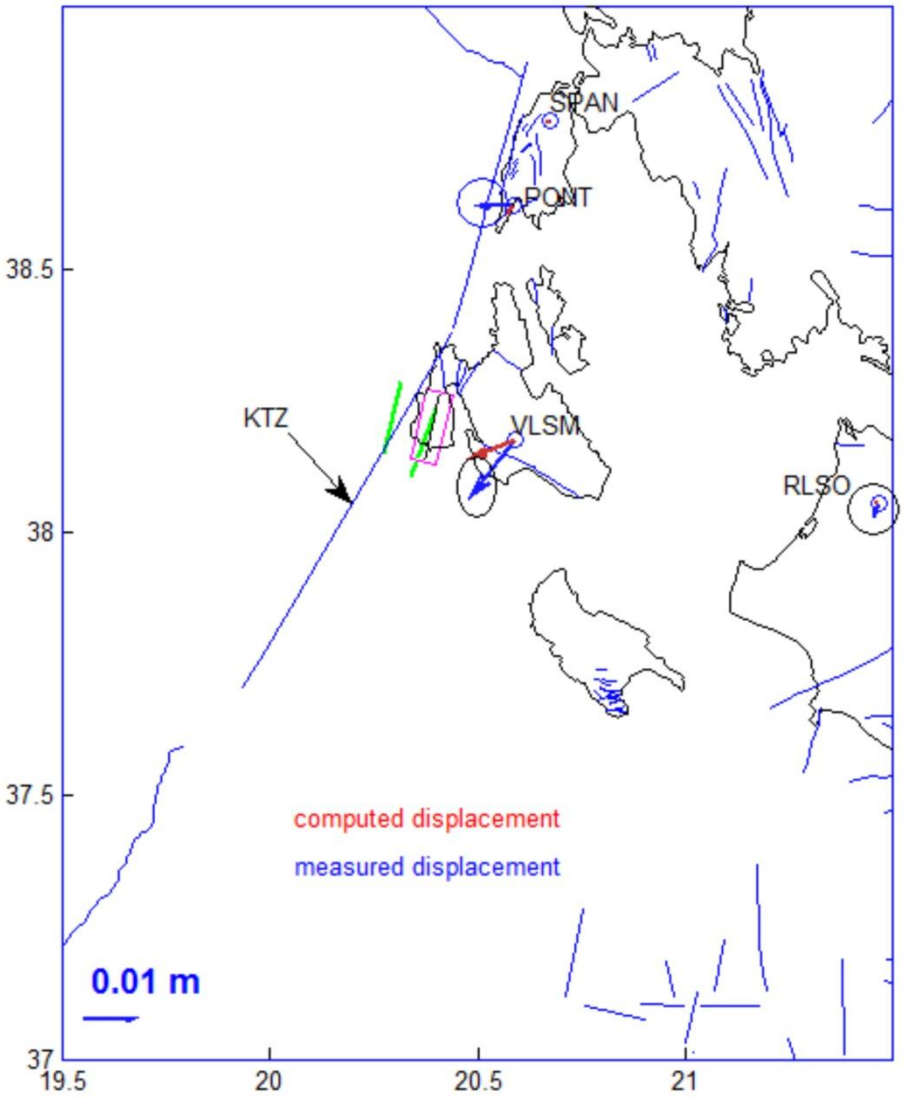

Figure 6. Measured (Table 1) and computed displacement at the surface, based on the INGV fault-plane solutions and the Okada model of dislocation in an elastic half-space. The red rectangles indicate the horizontal projection of the assumed fault planes. The green segments represent the intersection with the surface of the prolongation of the fault planes. Error ellipse represent 2D confidence at the 3σ level.

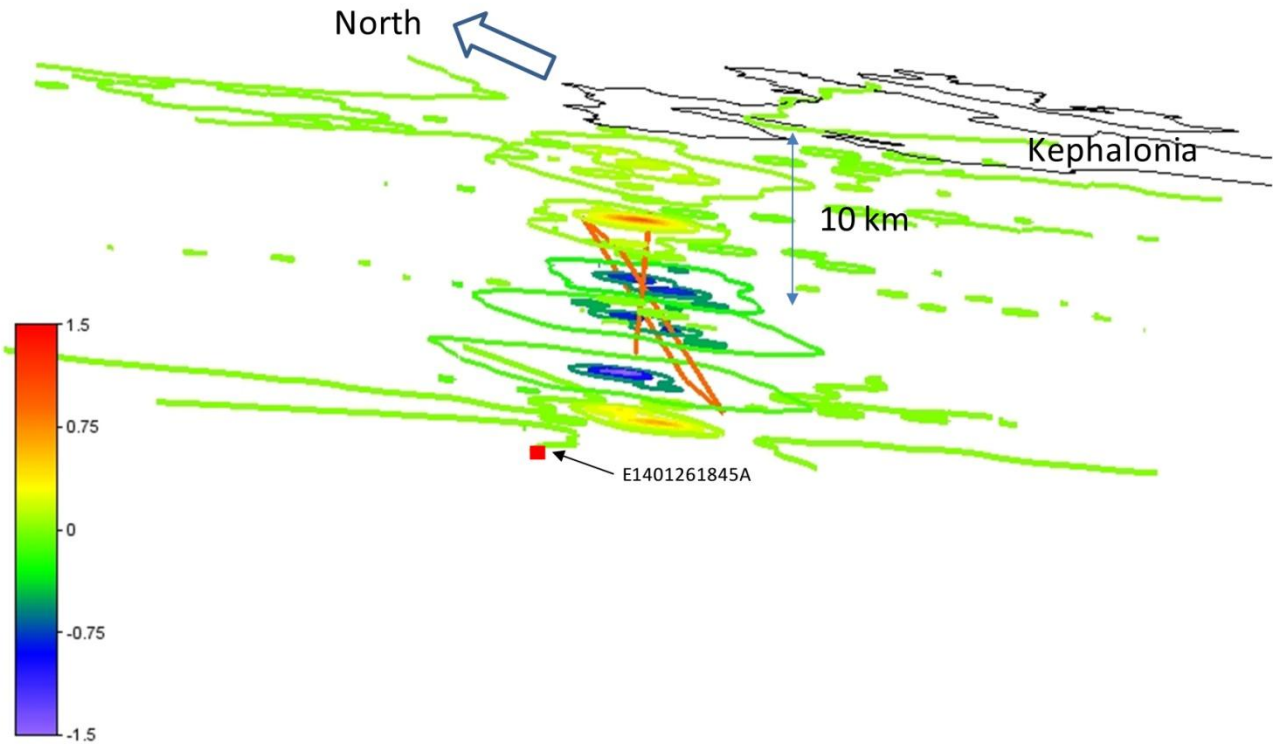

Figure 7. Coulomb stress change (MPa) following the Jan. 26 event (fault plane dips at 89°), computed on planes with the same orientation as that of the Feb. 03 event (dip =43°), at vertical steps of 3 km. Failure is promoted where the Coulomb change is more positive, hence very close to the top part of the failure plane of the Feb. 03 event. View angle is along the strike of the KTZ in NE direction. The red square indicates the hypocenter of the M_w=5.5 event which occurred some 5 hours after the Jan. 26 event.

(a)

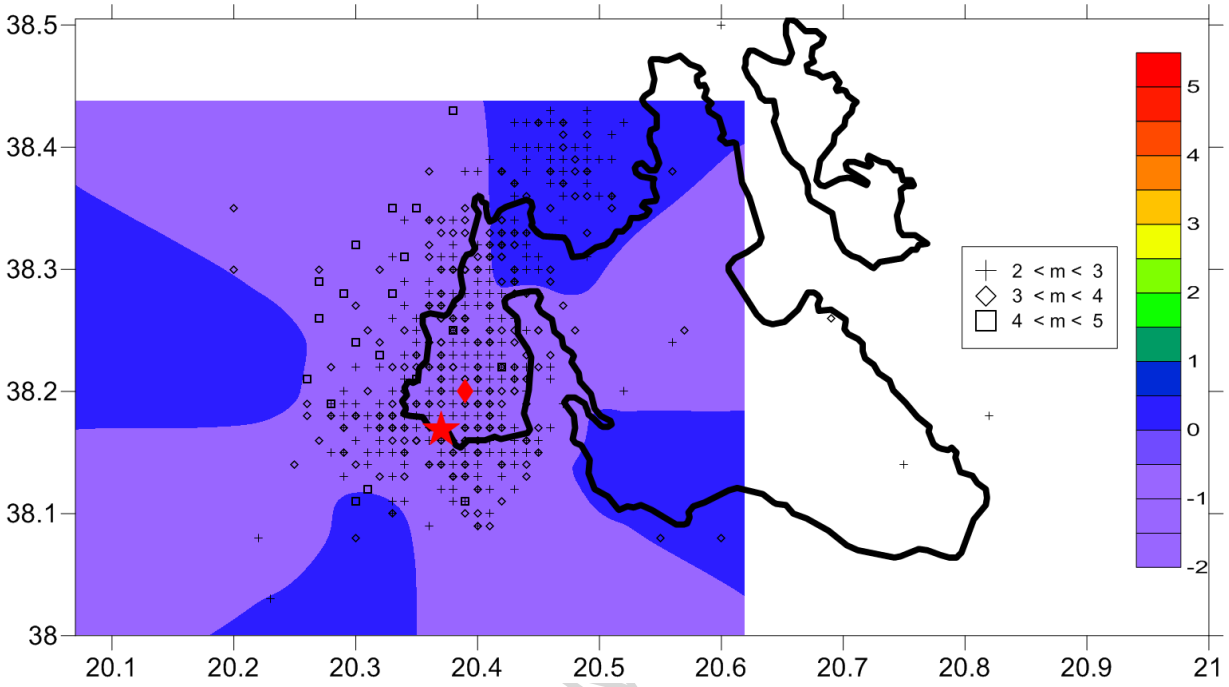

(b)

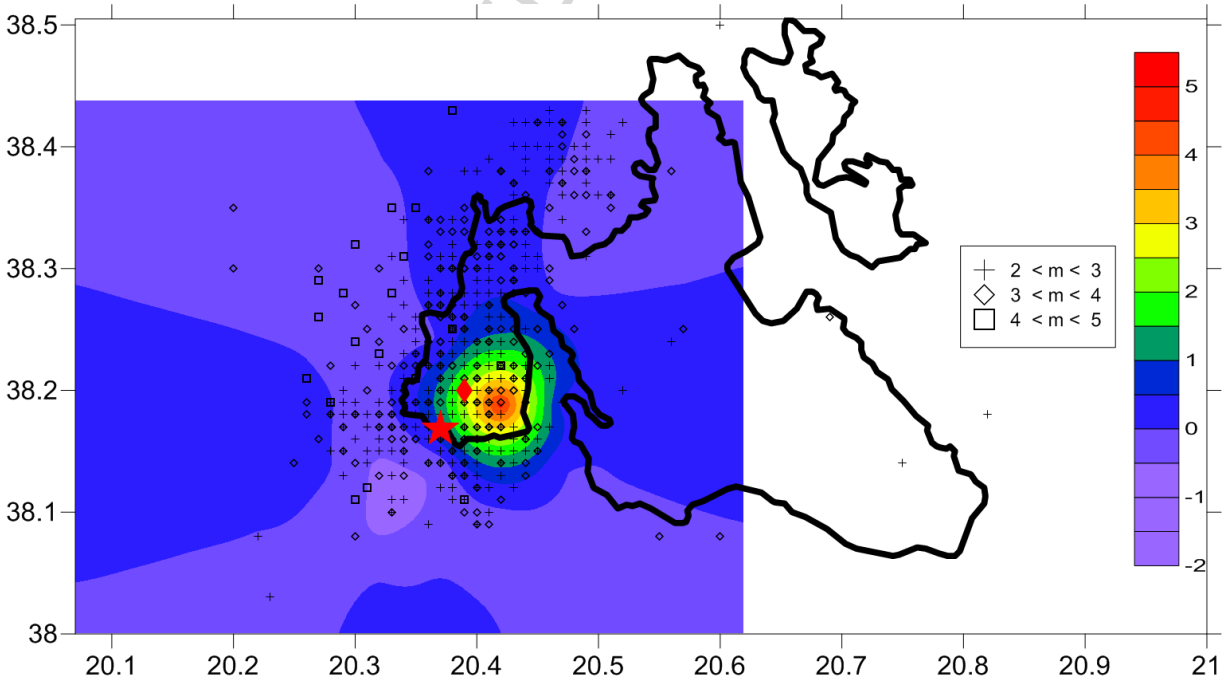

Figure 8. (a) Distribution of 1300 aftershocks up to Mar. 1, 2014 with contours of the Coulomb stress change on optimally oriented strike-slip planes, assuming a regional stress of 10 MPa (100 bar) oriented N65°E. (b) the regional stress is set at 0.4 MPa. The correlation between aftershocks and areas of positive Coulomb stress is more evident in b) than in a), where most of the aftershocks are located in a region of negative Coulomb stress change. Friction coefficient is f = 0.36. Color bar is in units of 1 MPa. Computation depth is 10 km. The star and diamond represent the epicenters of the January 26 and February 3 events, respectively.

Highlights

GPS strain rate, statistical seismicity and tectonics of the Kephalonia Transform Zone

A regional stress drop of 0.4-0.7 MPa is estimated

The Coulomb Failure Function for the events of 2014 yields the same regional stress

The regional stress very nearly balances the average stress released seismically